



*J. Serb. Chem. Soc.* 91 (0) 1–15 (2026)  
JSCS–13418

## Fabrication of visible-light photoactive TiO<sub>2</sub>/BiVO<sub>4</sub> composite for photocatalytic degradation of ciprofloxacin

THU LOAN DANG<sup>1</sup>, VU VAN TU<sup>2</sup>, THI HUE NGUYEN<sup>2</sup>, DUC VAN NGUYEN<sup>3\*</sup>  
and THI THAO TA<sup>1\*\*</sup>

<sup>1</sup>Faculty of Chemistry, VNU University of Science, 19 Le Thanh Tong, 100000, Vietnam,

<sup>2</sup>Institute of Science and Technology for Energy and Environment, Vietnam Academy of Science and Technology, 18 Hoang Quoc Viet, Nghia Do Ward, Hanoi 100000, Vietnam and

<sup>3</sup>Institute of Materials Science, Vietnam Academy of Science and Technology, 18 Hoang Quoc Viet, Nghia Do Ward, Hanoi 100000, Vietnam

(Received 13 June, revised 30 June, accepted 2 December 2025)

**Abstract:** Pure BiVO<sub>4</sub> and three TiO<sub>2</sub>/BiVO<sub>4</sub> composite photocatalysts with Bi<sup>3+</sup>:Ti<sup>4+</sup> mole ratios of 1:1, 2:1 and 4:1 were readily synthesized, for the first time, using a one-pot hydrothermal procedure for the photodegradation of ciprofloxacin. Conducting the hydrothermal reaction in a basic medium yielded single-phase scheelite monoclinic polymorphic BiVO<sub>4</sub> (ms-BiVO<sub>4</sub>) in the composite samples. Microstructural analysis showed spherical TiO<sub>2</sub> nanoparticles with an average grain size of 120 nm embedded on the surface of BiVO<sub>4</sub> nanoplates. The optimized composite exhibited a ciprofloxacin photodegradation reaction rate constant about 3.8 times higher than that of the pure BiVO<sub>4</sub> sample. This significant enhancement is attributed to the formation of a TiO<sub>2</sub>/BiVO<sub>4</sub> heterojunction, which promotes efficient charge separation. This research expands the knowledge on designing of BiVO<sub>4</sub>-rich composites (with Bi<sup>3+</sup>:Ti<sup>4+</sup> mole ratio ≥ 1:1) via heterogeneous junction engineering to enhance photocatalytic activity beyond that of pure BiVO<sub>4</sub>. The research also provided a perspective on using the BiVO<sub>4</sub>-rich composites as effective photocatalysts for degradation of antibiotics in aqueous media under visible-light irradiation.

**Keywords:** photocatalysis; semiconductor; heterojunctions; antibiotic residues; hydrothermal.

### INTRODUCTION

Over the last years, the widespread use of antibiotics in veterinary and human medicine has resulted in an increased risk for water contamination, as they are treated even at trace concentrations.<sup>1,2</sup> Particularly, it is estimated that many tons of antibiotic residues are released into the environment in Southeast Asia annually.<sup>3</sup> The

\*,\*\* Corresponding authors. E-mail: (\*)vannd@ims.vast.ac.vn; (\*\*)tathithao@hus.edu.vn  
<https://doi.org/10.2298/JSC250613001D>

World Health Organization (WHO) typically reports that pharmaceutical concentrations in surface waters, groundwater and partially treated water were below  $0.1 \mu\text{g L}^{-1}$  and concentrations in treated water were generally below  $0.05 \mu\text{g L}^{-1}$ .<sup>4</sup> The emerging environmental issue relating to antibiotic residues not only threatens public health but also compromises the effectiveness of the drugs themselves (*i.e.*, contributing to antibiotic resistance). Among the quinolone antibiotics class, ciprofloxacin (CFX) is widely utilized due to its broad-spectrum activity against many pathogenic bacteria. After medication, CFX can be partially broken down by metabolism in human or animal bodies and largely excreted in its pharmacologically active forms.<sup>5,6</sup> Therefore, practical and economical processes are urgently required to reduce the CFX antibiotic discharge into the environment.

To overcome this environmental challenge, various processes have been applied to degrade or remove contaminants, including adsorption, photocatalysis, biodegradation and electrochemical treatment.<sup>7</sup> While conventional treatments like filtration and coagulation/flocculation/sedimentation require subsequent procedure to treat the pollutants, other current techniques such as membrane, ozonation and Fenton process often bring weakness in the high costs of installation, investment and operation.<sup>1,8,9</sup> Consequently, photocatalytic semiconductors based on the advanced oxidation process (AOPs) are highly recommended. This technology is recognized largely as one of the most low-cost, sustainable and environmentally friendly approaches for wastewater treatment.<sup>10–13</sup>

Monoclinic bismuth orthovanadate ( $\text{BiVO}_4$ ), an *n*-type semiconductor, widely recognized as a promising solar-driven photocatalyst due to its narrow band gap (2.4 eV).  $\text{BiVO}_4$  exhibits outstanding features: nontoxic nature, high stability towards photocorrosion, low production cost, relatively strong oxidation properties for the decomposition of organic pollutants and its promising application as a photoanode material for water splitting. Nevertheless, the performance of the single component  $\text{BiVO}_4$  is still restricted by the fast recombination of photoinduced carriers (electron/hole pairs).<sup>14–17</sup> To date, various alternative strategies have been investigated to overcome limitation of  $\text{BiVO}_4$ , including cocatalyst loading, construction of heterostructures, and substitution of the metal cation or anion.<sup>18–22</sup> For the research approach of constructing heterostructures,  $\text{BiVO}_4$  was assembled with another semiconductor to form a heterojunction that can significantly reduce the combination and speed up the separation rate of photogenerated charge carriers.<sup>23–25</sup> To couple with  $\text{BiVO}_4$  to form these heterostructures, one of the most frequently-used semiconductors that serve as a second component is anatase titanium dioxide ( $\text{TiO}_2$ ) – a well-known photocatalyst with the band gap value of 3.2 eV to benefit its high chemical stability, and excellent photocatalytic activity.<sup>26–30</sup> Although numerous researches on  $\text{TiO}_2/\text{BiVO}_4$  photocatalytic composites have been reported, an optimized synthesis procedure has not been established. In addition, most published synthesis procedures of these photocatalytic

composites usually involve multi-steps, and to date, only limited number of one-pot approaches have been described in the literature.<sup>28,30</sup> Lv *et al.* applied one-pot hydrothermal procedure to synthesize TiO<sub>2</sub>/BiVO<sub>4</sub> nanocomposites with Bi<sup>3+</sup>:Ti<sup>4+</sup> mole ratios less than 0.2:1.<sup>28</sup> The photocatalytic efficiency of 60 % for photodegradation reaction of rhodamine B over the optimized sample after 4 h of visible-light irradiation. For TiO<sub>2</sub>/BiVO<sub>4</sub> system, to the best of our knowledge, TiO<sub>2</sub>-rich composites were studied the most,<sup>19,26–28,30</sup> while only one work focusing on BiVO<sub>4</sub>-rich composites with Bi<sup>3+</sup>:Ti<sup>4+</sup> mole ratio equals to or over 1:1 was reported.<sup>29</sup> However, the effects of Bi<sup>3+</sup>:Ti<sup>4+</sup> mole ratio on the photocatalytic efficiency of BiVO<sub>4</sub>-rich composites were not studied systematically by Drisya *et al.* for they only investigated Bi<sup>3+</sup>:Ti<sup>4+</sup> mole ratio value of 1:0.6. This might originate from the fact that these researches focused mainly on improving Vis-photocatalytic performances of TiO<sub>2</sub> *via* designing TiO<sub>2</sub>-based composites, in which BiVO<sub>4</sub> played role as a dopant or a minor component, rather than hindering the fast recombination of photoinduced electron-hole pairs, the main drawback of the pure BiVO<sub>4</sub>, *via* designing BiVO<sub>4</sub>-rich composites. In other words, the design of a heterogeneous junction to enhance photo-induced charge separation and consequently improve the photocatalytic performance of BiVO<sub>4</sub>-rich composites containing anatase as a minor component for photodegradation of antibiotics in general and CPX in particular, has not been mentioned yet.

Hence, this research aimed to synthesize TiO<sub>2</sub>/BiVO<sub>4</sub> semiconductors with Bi<sup>3+</sup>:Ti<sup>4+</sup> mole ratio equals to or greater than 1:1 using hydrothermal method in a basic medium, and their photocatalytic activities were determined by the degradation of CPX antibiotic in aqueous solution under visible-light irradiation.

## EXPERIMENTAL PROCEDURE

### *Synthesis of photocatalysts*

All the reagents were of analytical grade and used without any further purification. Typically, 1 mmol Bi(NO<sub>3</sub>)<sub>3</sub>·5H<sub>2</sub>O (Acros) and a certain amount of TiO<sub>2</sub> (Sigma–Aldrich) were dissolved in 2 mL of 4 M HNO<sub>3</sub> solution, while 1 mmol NH<sub>4</sub>VO<sub>3</sub> (Sigma–Aldrich) was dissolved in 10 mL double distilled water at 80 °C. The two solutions were mixed and transferred into a 120 mL Teflon<sup>®</sup>-lined stainless-steel autoclave. The pH of these mixtures was adjusted to 11 by addition of 12 mL of concentrated NH<sub>3</sub> solution (25 %). Subsequently, the autoclave was filled with double distilled water up to 75 % of its capacity. The sealed autoclave was heated at 180 °C for 24 h under autogenous pressure. After undergoing hydrothermal treatment, the precipitated solids were collected and washed with double distilled water until reaching a neutral medium. Finally, the yellow precipitates were obtained after drying naturally in air.

For the synthesis of the pure BiVO<sub>4</sub>, the same synthesis procedure was performed except that no TiO<sub>2</sub> was added. The three composite products were denoted as 1TiO<sub>2</sub>/4BiVO<sub>4</sub>, 1TiO<sub>2</sub>/2BiVO<sub>4</sub> and 1TiO<sub>2</sub>/1BiVO<sub>4</sub> corresponding to the sample with the Bi<sup>3+</sup>:Ti<sup>4+</sup> mole ratios of 4:1, 2:1 and 1:1, respectively.

### *Characterization methods*

The crystalline phases of the as-synthesized samples were determined by using an X-ray diffractometer (XRD, D8 Advance, Bruker). The synthesized samples were also characterized by field-emission scanning electron microscopy (FESEM, Hitachi S-4800), high resolution transmission electron microscopy (HR-TEM, Jeol 2100), and diffuse-reflectance UV-Vis spectrometry (DR-UV-Vis, Jasco V670).

### *Photocatalytic properties*

The photocatalytic activities of the studied composites were estimated by the degradation of ciprofloxacin (CPX) solution (0.5 ppm) at room temperature under visible-light irradiation. Typically, 0.025 g photocatalyst was added to 100 mL the antibiotic solution in each experiment. The solution was stirred for one hour in dark for reaching of adsorption-desorption equilibrium. The suspension was then irradiated by a visible-light source provided by a 100 W halogen lamp with the center wavelength of 700 nm from a distance of 20 cm. At certain interval times (30, 60, 90 and 120 min) during irradiation, 5 mL of the tested solution was taken out and was then filtrated with 0.22  $\mu\text{m}$  membrane prior to concentration determination by using a LC-MS/MS system (ACQUITY UPLC H-class/Xevo-TQ, USA).

The photocatalytic degradation efficiency was calculated by the following equation:

$$H = 100 \frac{C_0 - C_t}{C_0} \quad (1)$$

wherein:  $C_0$  is the initial concentration of CPX (without any photocatalyst);  $C_t$  is the remaining concentration of CPX in the solution at time  $t$  / min after irradiation.

## RESULTS AND DISCUSSION

### *Crystalline structure*

From XRD diagrams (Fig. 1), it can be confirmed that the monoclinic scheelite structure of  $\text{BiVO}_4$  (ms- $\text{BiVO}_4$ ) was successfully synthesized for all studied samples, namely, pure  $\text{BiVO}_4$ ,  $1\text{TiO}_2/4\text{BiVO}_4$ ,  $1\text{TiO}_2/2\text{BiVO}_4$  and  $1\text{TiO}_2/1\text{BiVO}_4$ . Particularly, diffraction peaks at  $2\theta$  values of 18.65, 18.98, 28.94, 30.54, 34.49, 35.22 and 39.78° are corresponding to (1 1 0), (0 1 1), (-1 3 0), (0 4 0), (2 0 0), (0 0 2) and (2 1 1) lattice planes of monoclinic scheelite structure of  $\text{BiVO}_4$  (JCPDS card No. 14-0688), respectively. Moreover, the doublet peaks at  $2\theta$  values of around 18.5 and 35° can be a useful mark to distinguish a monoclinic scheelite phase and a tetragonal scheelite phase of  $\text{BiVO}_4$ .<sup>31</sup>

The result indicated that, by carrying out the hydrothermal synthesis procedure in basic medium, the monoclinic scheelite structure was controlled to grow as a unique crystalline phase of  $\text{BiVO}_4$  and the coexistence of monoclinic scheelite and tetragonal zircon, as reported previously, was avoided.<sup>32</sup> In another word, the formation of tetragonal zircon phase, a thermodynamically stable polymorph of  $\text{BiVO}_4$  under the acidic medium of hydrothermal synthesis reaction, was totally inhibited.

In addition, for all XRD patterns of  $\text{TiO}_2/\text{BiVO}_4$  composite samples, a set of diffraction peaks at  $2\theta$  25.6, 38.3 and 48.8° were detected, indicating the existence

of anatase  $\text{TiO}_2$  (JCPDS card No. 21-1272).<sup>33</sup> Furthermore, no other impurity was found in all investigated samples, similar to those published for  $\text{TiO}_2/\text{BiVO}_4$  composites.<sup>28–30</sup> The intensity of anatase  $\text{TiO}_2$  increased monotonously as desirable with the  $\text{TiO}_2$  content in the composite samples when the  $\text{Bi}^{3+}:\text{Ti}^{4+}$  mole ratio decreased from 4:1 to 1:1. It is also worthy to note that by the coupling with anatase  $\text{TiO}_2$  to form photocatalytic composites, the calculated lattice parameters of the monoclinic scheelite  $\text{BiVO}_4$  existed in pure  $\text{BiVO}_4$ ,  $1\text{TiO}_2/4\text{BiVO}_4$ ,  $1\text{TiO}_2/2\text{BiVO}_4$  and  $1\text{TiO}_2/1\text{BiVO}_4$  samples were almost unchanged as tabulated in Table I.

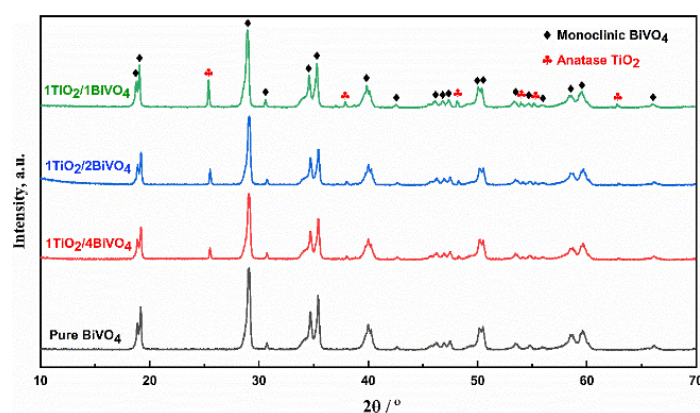


Fig. 1. XRD patterns of pure  $\text{BiVO}_4$  and  $\text{TiO}_2/\text{BiVO}_4$  composite samples.

TABLE I. The calculated lattice parameters ( $\text{\AA}$ ) of pure  $\text{BiVO}_4$ ,  $1\text{TiO}_2/4\text{BiVO}_4$ ,  $1\text{TiO}_2/2\text{BiVO}_4$  and  $1\text{TiO}_2/1\text{BiVO}_4$  samples

Sample	Lattice parameters			
	$a / \text{\AA}$	$b / \text{\AA}$	$c / \text{\AA}$	$\beta / ^\circ$
Pure $\text{BiVO}_4$	5.194(2)	11.699(2)	5.090(1)	90.38(1)
$1\text{TiO}_2/1\text{BiVO}_4$	5.195(1)	11.701(3)	5.089(2)	90.37(2)
$1\text{TiO}_2/2\text{BiVO}_4$	5.194(3)	11.700(2)	5.091(3)	90.38(2)
$1\text{TiO}_2/4\text{BiVO}_4$	5.194(1)	11.700(1)	5.092(2)	90.38(1)

### Microstructures

To investigate the morphology of the synthesized  $\text{TiO}_2/\text{BiVO}_4$  composite, the  $1\text{TiO}_2/4\text{BiVO}_4$  and  $1\text{TiO}_2/1\text{BiVO}_4$  samples were subjected to SEM observation as examples. The SEM image of the composite material, as shown in Figs. 2 and 3, reveals the presence of spherical-like  $\text{TiO}_2$  nanoparticles with the average grain size of 120 nm embedded on the surface of  $\text{BiVO}_4$  in contrast to that of the pure  $\text{BiVO}_4$ . This agrees well with the statement given for XRD patterns. For both cases of pure  $\text{BiVO}_4$  and  $\text{TiO}_2/\text{BiVO}_4$  composites, the  $\text{BiVO}_4$  nanoplates with average width of 200 nm and length of 300 nm are observed.

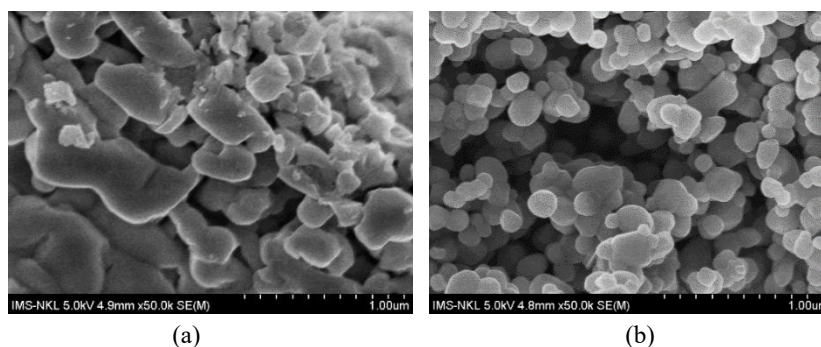


Fig. 2. SEM images of: a) pure BiVO<sub>4</sub> and b) 1TiO<sub>2</sub>/4BiVO<sub>4</sub> samples.

Compared to the case of commercialized TiO<sub>2</sub> precursor, the shape and average grain size TiO<sub>2</sub> nanoparticles existed in TiO<sub>2</sub>/BiVO<sub>4</sub> composite are almost unchanged, suggesting the inhibition role of basic medium on grain growth of TiO<sub>2</sub> (Fig. 3).<sup>34</sup>

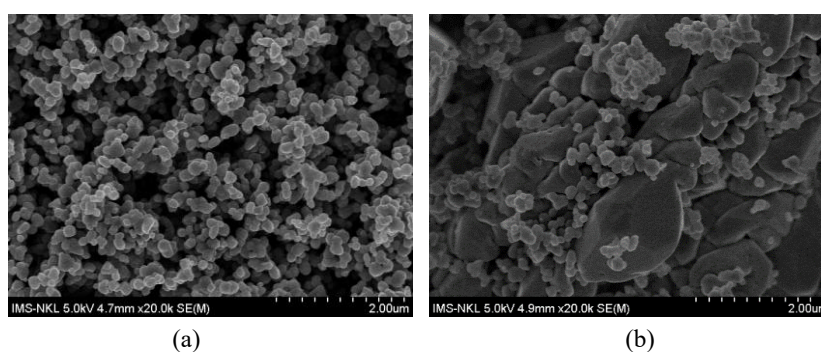


Fig. 3. SEM images of :a) commercialized TiO<sub>2</sub> precursor and b) 1TiO<sub>2</sub>/1BiVO<sub>4</sub> composite.

To investigate further the microstructure of as-synthesized samples, the HR-TEM image and its corresponding FFT pattern of 1TiO<sub>2</sub>/1BiVO<sub>4</sub> composite sample were presented in Fig. 4a and b, respectively. Two lattice fringe spacings of 0.292 and 0.467 nm with an interfacial angle of 66.5° that are assigned to (0 4 0) and (0 1 1) lattice planes of ms-BiVO<sub>4</sub>, respectively, were observed in both HR-TEM image and its corresponding FFT pattern. At the same time, two other lattice fringe spacings of 0.347 and 0.469 nm that formed an included angle of 68.3° were interpreted respectively as (0 1 1) and (0 0 2) lattice planes of anatase TiO<sub>2</sub> phase. These calculated results indicated obviously that the investigated 1TiO<sub>2</sub>/1BiVO<sub>4</sub> contained both ms-BiVO<sub>4</sub> and anatase TiO<sub>2</sub> particles. Moreover, as shown in Fig. 4a, the direct contact between ms-BiVO<sub>4</sub> nanoplates and anatase TiO<sub>2</sub> nanoparticles was observed, suggesting the formation of heterojunction between them.

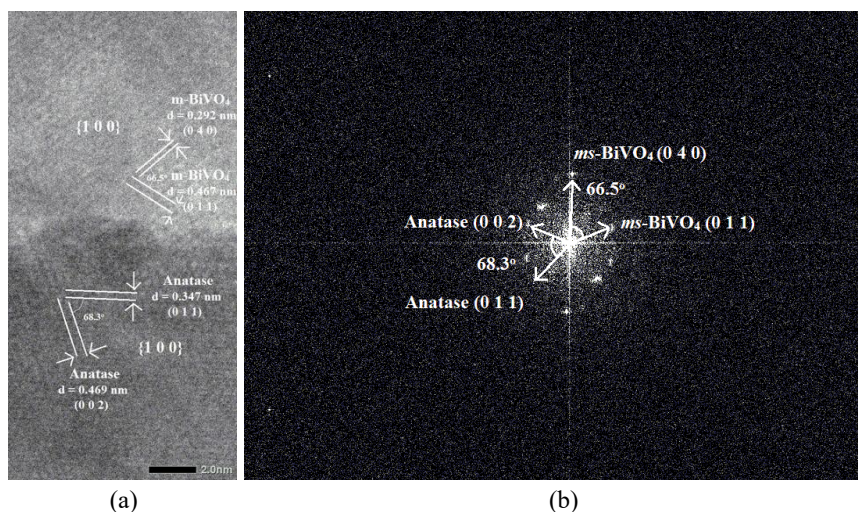


Fig. 4. a) HR-TEM image and b) its corresponding FFT pattern of  $1\text{TiO}_2/1\text{BiVO}_4$  composite sample.

#### Diffuse-reflectance (DR) UV-Vis spectra

From the spectra received by DR UV-Vis measurements as shown in Fig. 5, a derived Tauc's plot was then depicted in Fig. 6 that showed the relationship between  $h\nu$  (the energy of the light) and  $(\alpha h\nu)^2$ , where  $\alpha$  was the absorption coefficient of the material. Based on extrapolating the linear region in Fig. 6, the band gap ( $E_g$ ) values of synthesized photocatalysts were estimated to be 2.43, 2.42 and 2.44 eV, corresponding to the 4:1, 2:1 and 1:1 composite samples, respectively. The results showed the absorption feature of the composite materials and the pure  $\text{BiVO}_4$  as well ( $E_g = 2.42$  eV), in visible region, did not have a significant difference. Therefore, to conclude which as-prepared material was exhibiting the best photocatalytic activity, it was necessary to perform further photocatalytic tests with

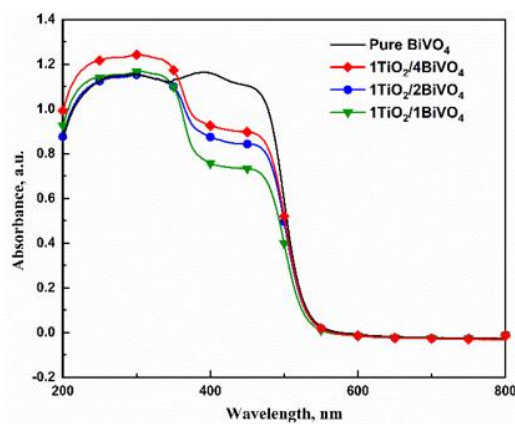


Fig. 5. Diffuse-reflectance UV-Vis spectra of pure  $\text{BiVO}_4$  and  $\text{BiVO}_4/\text{TiO}_2$  composites.

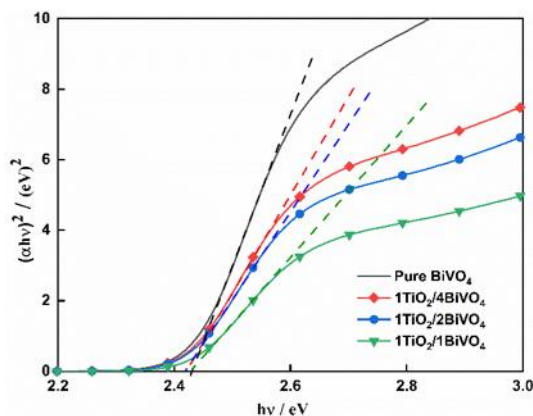


Fig. 6. Tauc's plots of pure  $\text{BiVO}_4$  and  $\text{BiVO}_4/\text{TiO}_2$  composites.

the analyte (*i.e.* ciprofloxacin (CFX)). However, the band gap values of around 2.4 eV suggested that photocatalytic experiments should be performed under visible-light irradiation.

#### Photocatalytic activities

Photocatalytic activities of as-synthesized samples were evaluated according to the degradation of CFX. These experiments included the photocatalytic degradation of only CFX solution without any photocatalyst; ciprofloxacin and pure  $\text{BiVO}_4$  (CFX+ $\text{BiVO}_4$ ); ciprofloxacin and 4:1 composite (CFX+ $1\text{TiO}_2/4\text{BiVO}_4$ ); and CFX and 1:1 composite (CFX+ $1\text{TiO}_2/1\text{BiVO}_4$ ). The photocatalytic degradation efficiency, after that, was illustrated in Fig. 7.

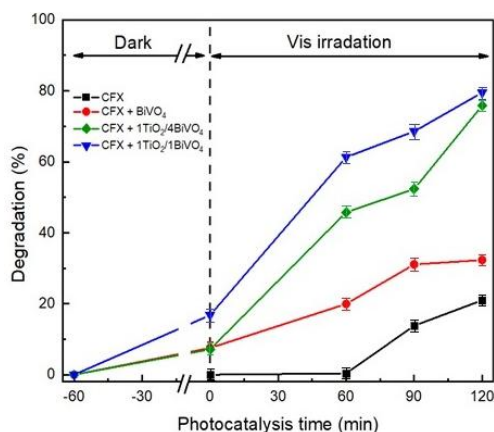


Fig. 7. Photocatalytic degradation efficiency of ciprofloxacin with and without the as-prepared photocatalysts under irradiation using a 100 W halogen lamp.

The results showed that after 120 min under visible-light irradiation, while CFX was degraded only 32 % in the activity of pure  $\text{BiVO}_4$ , but it was decomposed 75 and 80 % by  $1\text{TiO}_2/4\text{BiVO}_4$  and  $1\text{TiO}_2/1\text{BiVO}_4$ , respectively. Thus, similar to the previous works, the composite materials were visible-light photoactive with

their photodegradation efficiency obviously twice as high as that of the pure  $\text{BiVO}_4$  sample.<sup>19,23,28</sup> The existence of a heterojunction formed between  $\text{BiVO}_4$  nanoplates and embedded 120 nm spherical-like  $\text{TiO}_2$  nanoparticles can probably be attributed to this significant improvement in ciprofloxacin photodegradation efficiency of the studied  $\text{TiO}_2/\text{BiVO}_4$  composites with respect to that of the pure  $\text{BiVO}_4$ . Also, it can be derived from Fig. 7 that, after reaching of adsorption-desorption equilibrium, the CFX adsorption percentage of pure  $\text{BiVO}_4$  and  $1\text{TiO}_2/4\text{BiVO}_4$  samples was around 7 % and was almost the same while that of  $1\text{TiO}_2/1\text{BiVO}_4$  sample was higher (17 %). That can be explained by the fact that, the  $1\text{TiO}_2/1\text{BiVO}_4$  sample possessed the higher amount of spherical-like anatase  $\text{TiO}_2$  nanoparticles, with relatively high specific surface area (of around  $10 \text{ m}^2/\text{g}$ ), than pure  $\text{BiVO}_4$  and  $1\text{TiO}_2/4\text{BiVO}_4$  samples. In addition, the kinetics of the CFX photodegradation reactions over pure  $\text{BiVO}_4$  and  $1\text{TiO}_2/1\text{BiVO}_4$  samples was also investigated. The obtained results indicated that the CFX photodegradation reactions over these two samples can be described by the first-order kinetic equation (Fig. 8):

$$\ln(C_0 / C_t) = kt \quad (2)$$

where  $C_0$  is the initial CFX concentration,  $C_t$  is the CFX concentration at reaction time  $t$ , and  $k$  is the observed first-order rate constant. The photodegradation reaction rate constant of  $0.00899^\circ \text{ min}^{-1}$  calculated for the  $1\text{TiO}_2/1\text{BiVO}_4$  sample was about 3.8 times higher than that of the pure  $\text{BiVO}_4$  sample ( $0.00235^\circ \text{ min}^{-1}$ ) (Fig. 8, the inset).

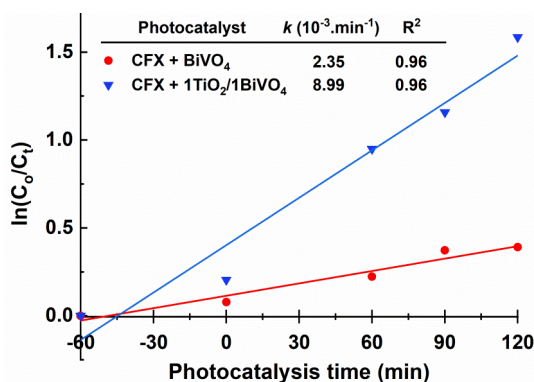
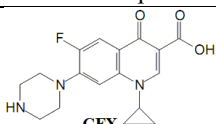
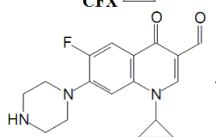
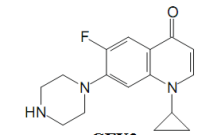


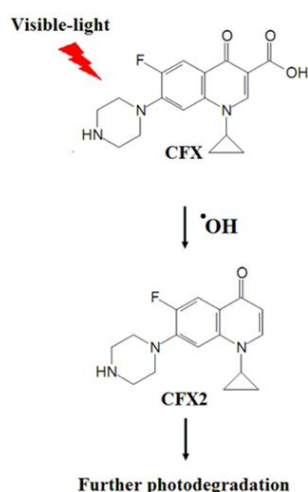
Fig. 8. The dependence of  $\ln(C_0/C_t)$  on the visible-light irradiation time of the optimized  $1\text{TiO}_2/1\text{BiVO}_4$  and the pure  $\text{BiVO}_4$  samples.

From  $m/z$  values obtained from LC-QTOFMS spectrum for the photodegradation of CFX over the optimized  $1\text{TiO}_2/1\text{BiVO}_4$  sample under visible-light irradiation, two major possible intermediate products, denoted as CFX1 and CFX2, were detected (Table II). The ion at  $m/z$  314.1 can be assigned to the dehydration of the CFX to produce CFX1.<sup>35</sup> The quinolone moiety of the CFX was attacked by the produced  $\bullet\text{OH}$  radicals, leading to a decarboxylation process to form CFX2 with  $m/z$  value of 288.1.<sup>36</sup> Based on these data, a CFX photocatalytic degradation

pathways under visible-light irradiation was proposed as shown in Scheme 1.<sup>36,37</sup> Accordingly, in a first step of the photodegradation reaction, CFX2 was formed as an intermediate product from the CFX under visible-light irradiation. By increasing the photocatalytic reaction time further, CFX2 was degraded into smaller substances. The photocatalytic reaction was completed when all available intermediate products of photodegradation reaction were mineralized into H<sub>2</sub>O and CO<sub>2</sub> as final compounds.<sup>36,37</sup>

TABLE II. Major *m/z* values and chemical formula of possible intermediate products detected by LC-MS/MS for the photodegradation of ciprofloxacin under visible-light irradiation

No.	Intermediate product	<i>m/z</i>	Possible chemical formula
1	 CFX	332.1	C <sub>17</sub> H <sub>18</sub> FN <sub>3</sub> O <sub>3</sub>
2	 CFX1	314.1	C <sub>17</sub> H <sub>17</sub> FN <sub>3</sub> O <sub>2</sub>
3	 CFX2	288.1	C <sub>16</sub> H <sub>18</sub> FN <sub>3</sub> O



Scheme 1. Proposed reaction pathways and intermediate products generated in the photodegradation reaction of ciprofloxacin under visible-light irradiation.

In Fig. 9 the recyclability testing results of CFX over the optimized 1TiO<sub>2</sub>/1BiVO<sub>4</sub> sample for three recycling photocatalytic runs under visible-light

irradiation are shown. The results illustrate that the photodegradation efficiency decreased slightly to 79.2 and 78.8 % for the second and third cycles, respectively from the value of 80 % for the first cycle. The CFX photodegraded species existing on the composite's surface might block the photoactive sites, leading to this slight decrease in photodegradation efficiency. This implied that our optimized  $\text{TiO}_2/\text{BiVO}_4$  composite sample can be reusable with high photocatalytic stability.

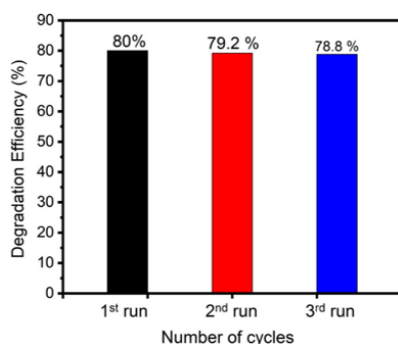


Fig. 9. Photodegradation recyclability test of ciprofloxacin over the optimized  $1\text{TiO}_2/1\text{BiVO}_4$  sample under visible-light irradiation.

Similar to the previous studies,<sup>27,38,39</sup> the photocatalytic activity-enhancing mechanism for CFX photodegradation in aqueous medium under visible-light irradiation over the  $\text{BiVO}_4$ -rich composites containing anatase as a minor component can be proposed as follows.

1) The incident light was absorbed mainly by the Vis-photoactive  $\text{BiVO}_4$  component of  $\text{TiO}_2/\text{BiVO}_4$  composite, leading to the generation of photo-induced pairs electron-hole pairs:



2) *Via* the heterojunction formed between  $m\text{s-BiVO}_4$  nanoplates and  $\text{TiO}_2$  nanoparticles, the photo-induced electrons in the conduction band of anatase  $\text{TiO}_2$  were transferred to that of  $\text{BiVO}_4$  while holes in the valence band of  $\text{BiVO}_4$  were transferred to that of anatase  $\text{TiO}_2$  under visible-light irradiation (Scheme 2).

3) The photo-induced charge transfer *via* heterojunction led to the increase in lifetime of electron-charge separation of the  $\text{TiO}_2/\text{BiVO}_4$  composites. This transfer was supposed to depend on the  $\text{Bi}^{3+}:\text{Ti}^{4+}$  mole ratio of this photocatalytic composite. The highest photocatalytic efficiency was found for the composite with the highest  $\text{Bi}^{3+}:\text{Ti}^{4+}$  mole ratio of 4:1 while the pure  $\text{BiVO}_4$  sample exhibited the fastest photo-induced charge recombination due to the absence of a charge transferring process. The further increase in  $\text{TiO}_2$  to decrease  $\text{Bi}^{3+}:\text{Ti}^{4+}$  mole ratio down to 1:1, however, lowered the composite's photocatalytic activity. This was probably due to multiple trapping of photo-induced charges.<sup>35</sup>

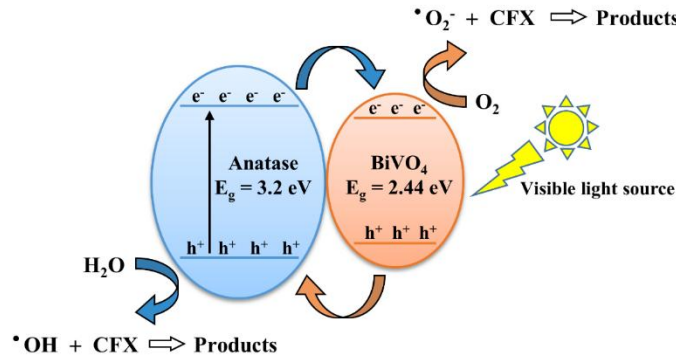
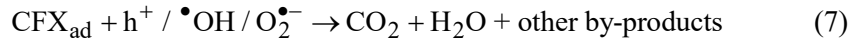
4) At the composite's surface, the dissolved oxygen in aqueous medium was oxidized by photo-induced electrons to active free radical species such as  $\text{O}_2^{\bullet-}$  and  $\bullet\text{OH}$ :



5) The electron donors ( $\text{H}_2\text{O}$ ) reacted with photo-induced holes at the composite's surface to produce  $\bullet\text{OH}$ :



6) The photo-induced holes and other freshly-produced free radicals like  $\text{O}_2^{\bullet-}$ ,  $\bullet\text{OH}$ , *etc.* oxidized the surface-adsorbed CFX ( $\text{CFX}_{\text{ad}}$ ) molecules to form photo-degraded species like  $\text{CO}_2$ ,  $\text{H}_2\text{O}$  and other by-products:



Scheme 2. The proposed photocatalytic mechanism of 1TiO<sub>2</sub>/1BiVO<sub>4</sub> sample for CFX photodegradation under visible-light irradiation.

## CONCLUSION

Pure BiVO<sub>4</sub> and three TiO<sub>2</sub>/BiVO<sub>4</sub> composite samples with mole ratios of 1:1, 2:1 and 4:1 were readily synthesized at a pH of 11 *via* hydrothermal method. Under the hydrothermal conditions, only a single-phase scheelite monoclinic polymorphic type of BiVO<sub>4</sub> (ms-BiVO<sub>4</sub>) was obtained, and the BiVO<sub>4</sub> nanoplates had average width of 200 nm and length of 300 nm.

Compared to the case of the pure BiVO<sub>4</sub>, the photocatalytic degradation rate of ciprofloxacin over the TiO<sub>2</sub>/BiVO<sub>4</sub> composites was significantly higher, and the 1TiO<sub>2</sub>/1BiVO<sub>4</sub> sample was expected to be the most potential photocatalyst with its highest efficiency of ciprofloxacin degradation after 120 min under visible-light irradiation. The enhancement in ciprofloxacin removal of the studied TiO<sub>2</sub>/BiVO<sub>4</sub>

composites might have originated from the existence of a heterojunction formed between BiVO<sub>4</sub> nanoplates and embedded 120 nm spherical-like TiO<sub>2</sub> nanoparticles.

## ИЗВОД

СИНТЕЗА TiO<sub>2</sub>/BiVO<sub>4</sub> КОМПОЗИТА ФОТОАКТИВНОГ НА ВИДЉИВУ СВЕЛОСТ ЗА ФОТОКАТАЛИТИЧКУ ДЕГРАДАЦИЈУ ЦИПРОФЛОКСАЦИНА

THU LOAN DANG<sup>1</sup>, VU VAN TU<sup>2</sup>, THI HUE NGUYEN<sup>2</sup>, DUC VAN NGUYEN<sup>3</sup> и THI THAO TA<sup>1</sup>

<sup>1</sup>Faculty of Chemistry, VNU University of Science, 19 Le Thanh Tong, 100000, Vietnam, <sup>2</sup>Institute of Science and Technology for Energy and Environment, Vietnam Academy of Science and Technology, 18 Hoang Quoc Viet, Nghia Do Ward, Hanoi 100000, Vietnam и <sup>3</sup>Institute of Materials Science, Vietnam Academy of Science and Technology, 18 Hoang Quoc Viet, Nghia Do Ward, Hanoi 100000, Vietnam

Чист BiVO<sub>4</sub> и три TiO<sub>2</sub>/BiVO<sub>4</sub> композитна фотокатализатора са молским односима Bi<sup>3+</sup>:Ti<sup>4+</sup> од 1:1, 2:1 и 4:1 успешно су синтетисани по први пут применом „one-pot“ хидротермалне процедуре за фотодеградацију ципрофлоксацина. Извођење хидротермалне реакције у базној средини резултирало је стварањем једнофазног моноклиничног BiVO<sub>4</sub> (ms-BiVO<sub>4</sub>) структуре шелита у узорцима композита. Микроструктурна анализа показала је сферичне наночестице TiO<sub>2</sub>, просечне величине зрна од 120 nm, које су уграђене на површину наноплоча BiVO<sub>4</sub>. Оптимизовани композит показао је константу брзине реакције фотодеградације ципрофлоксацина која је била око 3.8 пута већа у поређењу са узорком чистог BiVO<sub>4</sub>. Ово значајно побољшање приписује се формирању TiO<sub>2</sub>/BiVO<sub>4</sub> хетероједињења које поспешује ефикасно раздвајање наелектрисања. Ово истраживање проширује знање о дизајнирању композита богатих са BiVO<sub>4</sub> (са молским односом Bi<sup>3+</sup>:Ti<sup>4+</sup> ≥ 1:1) путем инжењеринга хетерогених спојева ради побољшања фотокаталитичке активности изнад нивоа чистог BiVO<sub>4</sub>. Истраживање је такође пружило перспективу о коришћењу композита богатих BiVO<sub>4</sub> као ефикасних фотокатализатора за деградацију антибиотика у воденим растворима, под зрачењем видљивом светлошћу.

(Примљено 13. јуна, ревидирано 30. јуна, прихваћено 2. децембра 2026)

## REFERENCES

1. V. Homem, L. Santos, *J. Environ. Manage.* **92** (2011) 2304 (<https://doi.org/10.1016/j.jenvman.2011.05.023>)
2. C. Yan, Y. Yang, J. Zhou, M. Liu, M. Nie, H. Shi, L. Gu, *Environ. Pollut.* **175** (2013) 22 (<https://doi.org/10.1016/j.envpol.2012.12.008>)
3. C. S. Lundborg, A. Tamhankar, *BMJ.* **358** (2017) j2440 (<https://doi.org/10.1136/bmj.j2440>)
4. *Pharmaceuticals in drinking-water*, World Health Organization, Geneva, 2012, p. 35 (<https://apps.who.int/iris/handle/10665/44630>)
5. S. Babić, M. Periša, I. Škorić, *Chemosphere* **91** (2013) 1635 (<https://doi.org/10.1016/j.chemosphere.2012.12.072>)
6. J. Porras, C. Badoya, J. Silva-Agreedo, A. Santamaría, J. J. Fernández, R. A. Torres-Palma, *Water Res.* **94** (2016) 1 (<https://doi.org/10.1016/j.watres.2016.02.024>)
7. Z. Wei, J. Liu, W. Shangguan, *Chinese J. Catal.* **41** (2020) 1440 ([https://doi.org/10.1016/S1872-2067\(19\)63448-0](https://doi.org/10.1016/S1872-2067(19)63448-0))
8. K. Košutić, D. Dolar, D. Ašperger, B. Kunst, *Sep. Purif. Technol.* **53** (2007) 244 (<https://doi.org/10.1016/j.seppur.2006.07.015>)

9. C. A. Igwegbe, S. N. Oba, C. O. Aniagor, A. G. Adeniyi, *Ind. Eng. Chem. Res.* **93** (2021) 57 (<https://doi.org/10.1016/j.jiec.2020.09.023>)
10. M. N. Chong, B. Jin, C. W. K. Chow, C. Saint, *Water Res.* **44** (2010) 2997 (<https://doi.org/10.1016/j.watres.2010.02.039>)
11. S. Dong, J. Feng, M. Fan, Y. Pi, L. Hu, X. Han, M. Liu, J. Sun, J. Sun, *RSC Adv.* **5** (2015) 14610 (<https://doi.org/10.1039/C4RA13734E>)
12. W. S. Koe, J. W. Lee, W. C. Chong, Y. L. Pang, L. C. Sim, *Environ. Sci. Pollut.* **27** (2020) 2522 (<https://doi.org/10.1007/s11356-019-07193-5>)
13. S. Zhu, D. Wang, *Adv. Energy Mater.* **7** (2017) 1700841 (<https://doi.org/10.1002/aenm.201700841>)
14. A. Malathi, J. Madhavan, M. Ashokkumar, P. Arunachalam, *Appl. Catal., A* **555** (2018) 47 (<https://doi.org/10.1016/j.apcata.2018.02.010>)
15. M. Guo, Q. He, A. Wang, W. Wang, Z. Fu, *Crystals* **6** (2016) 81 (<https://doi.org/10.3390/cryst6070081>)
16. O. Monfort, G. Plesch, *Environ. Sci. Pollut.* **25** (2018) 19362 (<https://doi.org/10.1007/s11356-018-2437-9>)
17. H. L. Tan, R. Amal, Y. H. Ng, *J. Mater. Chem., A* **5** (2017) 16498 (<https://doi.org/10.1039/C7TA04441K>)
18. Y. Li, D. Liao, T. Li, W. Zhong, X. Wang, X. Hong, H. Yu, *J. Colloid Interface Sci.* **570** (2020) 232 (<https://doi.org/10.1016/j.jcis.2020.02.093>)
19. S. Obregón, G. Colón, *RSC Adv.* **4** (2014) 6920 (<https://doi.org/10.1039/c3ra46603e>)
20. X.-J. Wen, C. G. Niu, L. Zhang, C. Liang, H. Guo, G. M. Zeng, *J. Catal.* **358** (2018) 141 (<https://doi.org/10.1016/j.jcat.2017.11.029>)
21. B. Zhang, H. Zhang, Z. Wang, X. Zhang, X. Qin, Y. Dai, Y. Liu, P. Wang, Y. Li, B. Huang, *Appl. Catal.* **211** (2017) 258 (<https://doi.org/10.1016/j.apcatb.2017.03.078>)
22. D. B. Hernández-Uresti, C. Alanis-Moreno, D. Sanchez-Martinez, *Mater. Sci. Semicond.* **102** (2019) 104585 (<https://doi.org/10.1016/j.mssp.2019.104585>)
23. K. Pingmuang, J. Chen, W. Kangwansupamonkon, G. G. Wallace, S. Phanichphant, A. Nattestad, *Sci. Rep.* **7** (2017) 8929 (<https://doi.org/10.1038/s41598-017-09514-5>)
24. Z. Ye, X. Xiao, J. Chen, Y. Wang, *Photochem. Photobiol., A* **368** (2018) 153 (<https://doi.org/10.1016/j.jphotochem.2018.09.044>)
25. J. Yang, Q. Shi, R. Zhang, M. Xie, X. Jiang, F. Wang, X. Cheng, W. Han, *Carbon* **138** (2018) 118 (<https://doi.org/10.1016/j.carbon.2018.06.003>)
26. Y. Hu, W. Chen, J. Fu, M. Ba, F. Sun, P. Zhang, J. Zou, *App. Surf. Sci.*, **436** (2018) 319 (<https://doi.org/10.1016/j.apsusc.2017.12.054>)
27. W. Li, Z. Wang, D. Kong, D. Du, M. Zhou, Y. Du, T. Yan, J. You, D. Kong, *J. Alloys Compd.* **688** (2016) 703 (<http://dx.doi.org/10.1016/j.jallcom.2016.07.249>)
28. Y.-R. Lv, C.-J. Liu, R.-K. He, X. Li, Y.-H. Xu, *Mater. Res. Bull.* **117** (2019) 35 (<https://doi.org/10.1016/j.materresbull.2019.04.032>)
29. K. T. Drisya, M. Solís-López, J. J. Ríos-Ramírez, J. C. Durán-Álvarez, A. Rousseau, S. Velumani, R. Asomoza, A. Kassiba, A. Jantrania, H. Castaneda, *Sci. Rep.* **10** (2020) 13507 (<https://doi.org/10.1038/s41598-020-69032-9>)
30. G. Longo, F. Fresno, S. Gross, U. L. Štangar, *Environ. Sci. Pollut. Res.* **21** (2014) 11189 (<https://doi.org/10.1007/s11356-014-2624-2>)
31. S. Okunaka, H. Tokudome, Y. Hitomi, R. Abe, *J. Mater. Chem., A* **4** (2016) 3926 (<https://doi.org/10.1039/C5TA09789D>)

32. Y. Zhou, G. Jiang, R. Wang, X. Wang, R. Hu, X. Xi, *J. Fiber Bioeng. Inform.* **5** (2012) 181 (<https://doi.org/10.3993/jfbi06201207>)
33. L. Zhang, G. Tan, S. Wei, H. Ren, A. Xia, Y. Luo, *Ceram. Int.* **39** (2013) 8597 (<https://doi.org/10.1016/j.ceramint.2013.03.106>)
34. D. Li, H. Song, X. Meng, T. Shen, J. Sun, W. Han, X. Wang, *Nanomaterials (Basel)* **10** (2020) 546 (<https://doi.org/10.3390/nano10030546>)
35. M. Jiménez-Salcedo, M. Monge, M. T. Tena, *Chemosphere* **247** (2020) 125910 (<https://doi.org/10.1016/j.chemosphere.2020.125910>)
36. T. Ahamad, M. Naushad, S. M. Alshehri, *Chem. Eng. J.* **417** (2021) 127969 (<https://doi.org/10.1016/j.cej.2020.127969>)
37. T. G. Vasconcelos, D. M. Henriques, A. König, A. F. Martins, K. Kümmerer, *Chemosphere* **76** (2009) 487 (<https://doi.org/10.1016/j.chemosphere.2009.03.022>)
38. Y. Kang, Y. Yang, L.-C. Yin, X. Kang, G. Liu, H.-M. Cheng, *Adv. Mater.* **27** (2015) 4572 (<https://doi.org/10.1002/adma.201501939>)
39. N. D. Van, D. T. A. Thu, N. T. H. Le, Do. T. Anh, *Mater. Sci. Eng., B* **278** (2022) 115616 (<https://doi.org/10.1016/j.mseb.2022.115616>).